

**NASA
Technical
Paper
2556**

1986

Hydroburst Test of a Carbon-Carbon Involute Exit Cone

Roy M. Sullivan

*George C. Marshall Space Flight Center
Marshall Space Flight Center, Alabama*

NASA

National Aeronautics
and Space Administration

**Scientific and Technical
Information Branch**

TABLE OF CONTENTS

	Page
I. INTRODUCTION	1
A. Purpose	1
B. Summary	1
II. BUCKLING TEST	2
A. Test Specimen	2
B. Test Fixture	2
C. Instrumentation	4
D. Test Procedure	4
E. Test Results	6
III. SPAR FINITE ELEMENT MODEL	23
IV. DISCUSSION	26
V. CONCLUSIONS	27
REFERENCES	28

PRECEDING PAGE BLANK NOT FILMED

PRECEDING PAGE BLANK NOT FILMED

LIST OF ILLUSTRATIONS

Figure	Title	Page
1.	Test fixture	2
2.	Fixed-fixed test specimen	3
3.	Plastic sheathing encompassing entire cone exterior	3
4.	Illustration of strain gage locations	5
5.	Failed cone	6
6.	Circumferential strains recorded by uniaxial gages plotted against applied pressure	7
7.	Inside/outside axial strain at 5-3/8 in. and 60 deg plotted against applied pressure	8
8.	Inside/outside axial strain at 5-3/8 in. and 180 deg plotted against applied pressure	9
9.	Inside/outside axial strain at 5-3/8 in. and 300 deg plotted against applied pressure	10
10.	Inside/outside axial strain at 13-1/8 in. and 60 deg plotted against applied pressure	11
11.	Inside/outside axial strain at 13-1/8 in. and 180 deg plotted against applied pressure . . .	12
12.	Inside/outside axial strain at 13-1/8 in. and 300 deg plotted against applied pressure . . .	13
13.	Inside/outside circumferential strain at 5-3/8 in. and 60 deg plotted against applied pressure	14
14.	Inside/outside circumferential strain at 5-3/8 in. and 180 deg plotted against applied pressure	15
15.	Inside/outside circumferential strain at 5-3/8 in. and 300 deg plotted against applied pressure	16
16.	Inside/outside circumferential strain at 9-7/8 in. and 0 deg plotted against applied pressure	17
17.	Inside/outside circumferential strain at 9-7/8 in. and 120 deg plotted against applied pressure	18
18.	Inside/outside circumferential strain at 9-7/8 in. and 240 deg plotted against applied pressure	19
19.	Inside/outside circumferential strain at 13-1/8 in. and 60 deg plotted against applied pressure	20

LIST OF ILLUSTRATIONS (Concluded)

Figure	Title	Page
20.	Inside/outside circumferential strain at 13-1/8 in. and 180 deg plotted against applied pressure.	21
21.	Inside/outside circumferential strain at 13-1/8 in. and 300 deg plotted against applied pressure.	22
22.	Constructed SPAR model	23
23.	SPAR model applied loading.	24
24.	Analytical buckling load	24
25.	Predicted buckling mode (axial view)	25
26.	Predicted buckling mode (side view)	25

LIST OF TABLES

Table	Title	Page
1.	Description of Strain Gage Locations	5
2.	Circumferential and Axial Element Stresses Due to the Critical Applied Pressure	26
3.	Measured and Predicted Circumferential Strain Comparison at Various Cone Locations	27

TECHNICAL PAPER

HYDROBURST TEST OF A CARBON-CARBON INVOLUTE EXIT CONE

I. INTRODUCTION

A. Purpose

On December 20, 1984, a sea-level test firing of the PAM-D motor (CCT-1) was conducted at Elkton Thiokol, Elkton, Maryland. During the firing, the PAM-D exit cone failed catastrophically. Afterwards, it was concluded that a net external pressure, due to the sea-level air pressure, buckled the aft portion of the carbon-carbon exit cone. As a result, a buckling analysis of the PAM-D exit cone using the SPAR finite element code was performed by the Stress Analysis Branch, EP46, at MSFC.

The theoretical analysis is not complete without a material correlation or knockdown factor. The correlation factor accounts for material imperfections and variations in the carbon-carbon material properties. This correlation factor was achieved with the aid of a hydrostatic buckling test of the aft end of the PAM-D exit cone. A SPAR buckling analysis that simulates the hydrostatic test conditions produced a theoretical critical pressure, and then a comparison between the measured and predicted values resulted in a material knockdown factor. The knockdown factor will adjust the SPAR buckling analysis of the next sea-level firing of the PAM-D motor (CCT-2).

The immediate objective of this test was to obtain the critical pressure to induce buckling of the aft end of the PAM-D exit cone. However, since the second sea-level firing of the PAM-D motor (CCT-2) was postponed, additional time was available for strain gage instrumentation of the test specimen. The addition of strain data allowed a check on the modulus of elasticity chosen for the finite element model as well as determined if the cone failure was due to buckling or stress failure.

This report describes the hydrostatic buckling test and presents the recorded data. The analytical model is then explained and the model results are presented. Subsequently, in order to determine the material correlation factor, the results are evaluated and comparisons are made between the measured and predicted values.

B. Summary

A hydrostatic buckling test was conducted by the Test Laboratory at MSFC on March 18, 1985. Strains at various locations were recorded for each applied pressure. The applied pressure required for elastic cone buckling was 9.75 psi.

A SPAR finite element model was constructed which simulated the test conditions. A buckling pressure was computed by an eigenvalue solution and then stresses induced by the buckling pressure were computed by a SPAR stress solution. The SPAR model calculated an applied buckling pressure of 8.76 psi.

A material correlation factor for the carbon-carbon exit cone was determined by comparing measured and predicted values of the critical pressures. The correlation factor based on the critical pressures was 1.1. This provides confidence in the SPAR model accuracy, since the correlation factor is near unity. Consequently, this provides confidence in a SPAR buckling analysis of the CCT-2 where a similar modeling scheme is used.

II. BUCKLING TEST

ORIGINAL PAGE IS
OF POOR QUALITY

The test fixture was fabricated and the testing was conducted at the MSFC Test Laboratory under the supervision of Mr. David Snoddy, ET52.

A. Test Specimen

The test specimen was a 14.875-in. segment of the aft end of the PAM-D exit cone. Its diameter ranged from 20.6875 in. to 29.5 in. A stiffening ring at approximately mid-height of the cone increased the cone stiffness.

B. Test Fixture

The test fixture (Fig. 1) was a cylindrical steel pressure vessel with a 33.0-in. diameter and a 25.0-in. depth. Pressure was applied to the vessel with a Pacco hand-loader, serial number 30087-1. A mechanical pressure gage allowed visual inspection of the applied pressure, and an electronic pressure gage recorded the applied pressure along with the strain data.

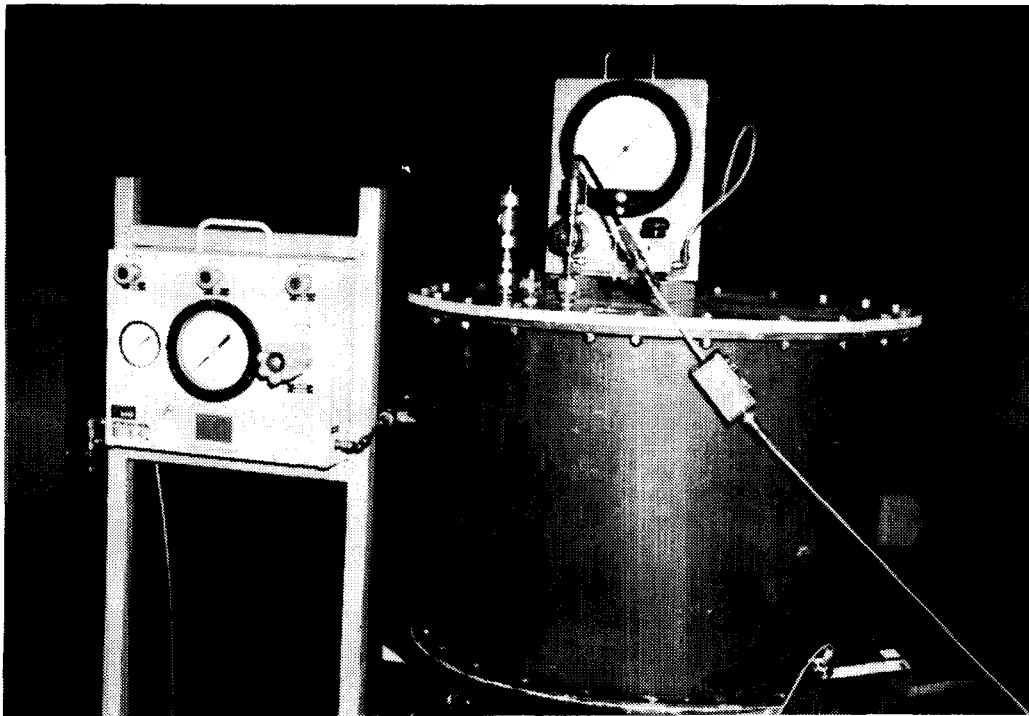


Figure 1. Test fixture.

It was essential that the geometry, boundary conditions, and loading of the SPAR model simulated that of the test configuration, so that the difference between the measured and predicted buckling pressure could be attributed solely to the material property variations. The pressure loading and cone geometry are easily modeled with the SPAR program. However, the SPAR code allows only "fixed" and/or "free" boundary conditions. As a result, a fixed-fixed boundary condition was chosen for the test

configuration, since it was the easiest to fabricate and correlate with a SPAR model. The base of the cone was fixed to the vessel base by epoxy and the top of the cone was fixed by epoxy to a metal bridge (Fig. 2). This ensured a fixed-fixed boundary condition as well as prevented water flow into the cone.

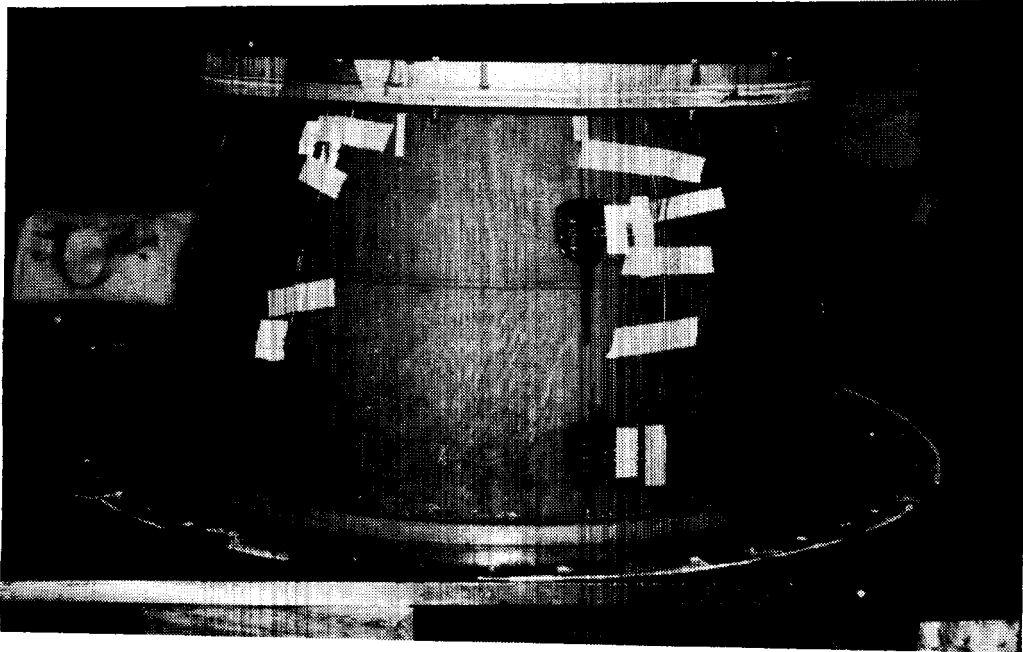


Figure 2. Fixed-fixed test specimen.

Since the carbon-carbon material properties are affected by moisture, a plastic sheathing with no load carrying capability encompassed the entire external cone area and prevented the carbon-carbon material from becoming saturated (Fig. 3).

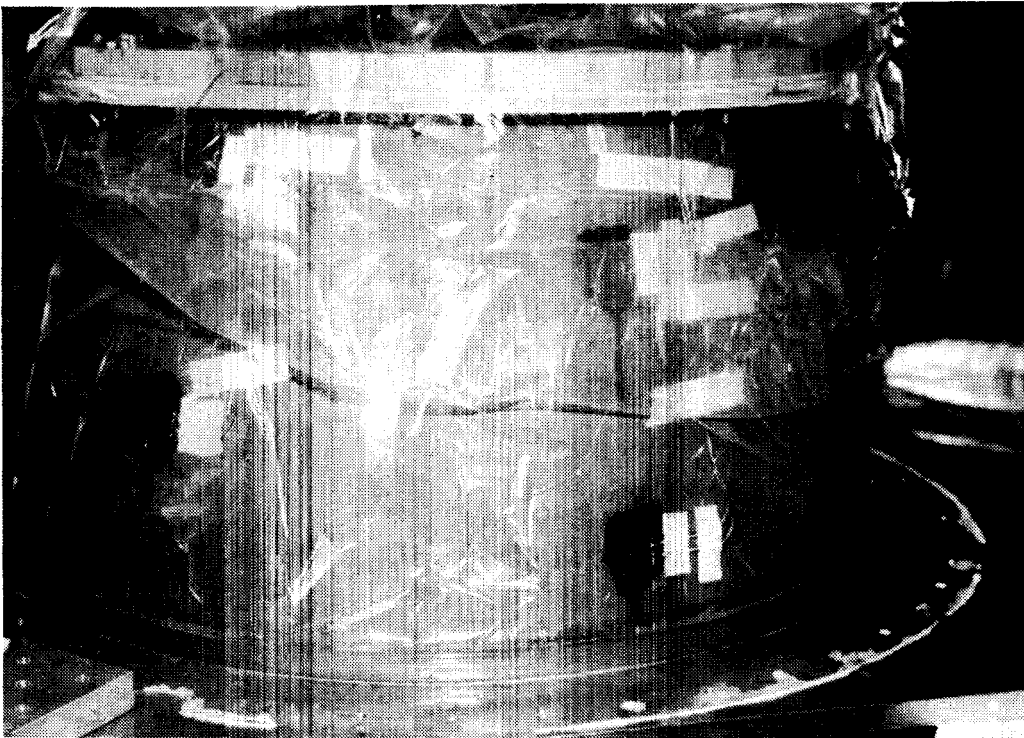


Figure 3. Plastic sheathing encompassing entire cone exterior.

The metal bridge carried the axial load resulting from pressurization. This is significant since cone buckling is affected by an axial loading.

Three openings in the vessel base provided an exit for the strain gage lead wires as well as provided a means for water discharge at the completion of the test. These openings also allowed the cone interior to remain at ambient air pressure, so that the net external pressure loading was the water head plus any applied pressure from the hand-loader.

C. Instrumentation

The exit cone was instrumented by the Materials Laboratory at MSFC with uniaxial, biaxial, and triaxial strain gages. Four uniaxial gages measured circumferential strains on the inside surface at a height of 7 in. below the top of the cone.

Biaxial gages measured circumferential and axial strains on the inside and outside surfaces (back-to-back) at four cone heights and at various circumferential locations. A strain variation around the circumferential would detect plastic buckling, if it were to occur. Triaxial gages measured strains at two cone heights and at five circumferential locations. A pretest ultrasound inspection located the areas where material properties were critical and triaxial gages were placed at these critical locations.

Mr. Ben Goldberg, EH34, installed the strain gages and conducted the material testing.

An Acurex System (Autodata 1050, Acurex Corp., Mt. View, California) recorded the strain data along with the applied pressure.

Table 1 identifies and Figure 4 illustrates the strain gage locations for the uniaxial and biaxial locations.

D. Test Procedure

The pressure vessel was filled with water at room temperature, so that initially a linearly varying pressure profile, due to the water head, was applied to the cone exterior. Air pressure was then applied to the water filled vessel with the hand-loader. The resultant pressure loading could then be adjusted by the hand-loader setting.

Starting at zero applied air pressure and continuing until cone failure, strain data were recorded for each 0.5 psi increment of applied air pressure. A loading rate of 0.5 psi approximately every 20 sec ensured a static loading condition as well as permitted a complete scan of the strain data for each load step.

The cone failure occurred at an applied air pressure of 9.75 psi. This corresponds to a resultant pressure profile which varies linearly and ranges from 10.10 psi ($0.35 + 9.75$) at the top of the cone to 10.65 psi ($0.9 + 9.75$) at the base of the cone, due to the applied pressure plus head pressure.

At failure, the pressure profile was lost due to a complete collapse of one section of the cone (Fig. 5).

TABLE 1. DESCRIPTION OF STRAIN GAGE LOCATIONS

Uniaxial – all gages at 7 in. from top of cone circumferential location.

- U1 0°
- U2 90°
- U3 180°
- U4 270°

Biaxial – inside and outside gages are back-to-back.

Outside:

Height	0°	60°	120°	180°	240°	300°
2-1/4 in.	01		05		09	
5-3/8 in.		03		07		011
9-7/8 in.	02		06	013	010	
13-1/8 in.		04		08		012

Inside:

Height	0°	60°	120°	180°	240°	300°
2-1/4 in.	11		15		19	
5-3/8 in.		13		17		111
9-7/8 in.	12		16		110	
13-1/8 in.		14		18		112

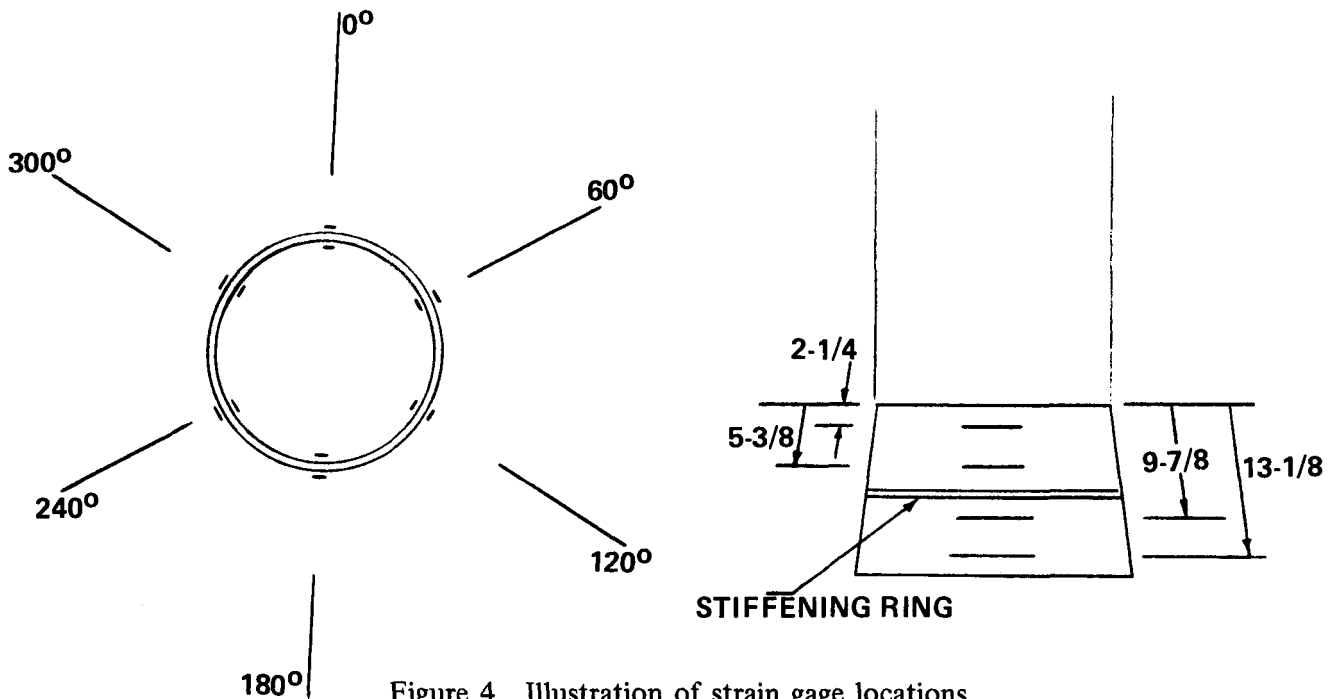


Figure 4. Illustration of strain gage locations.

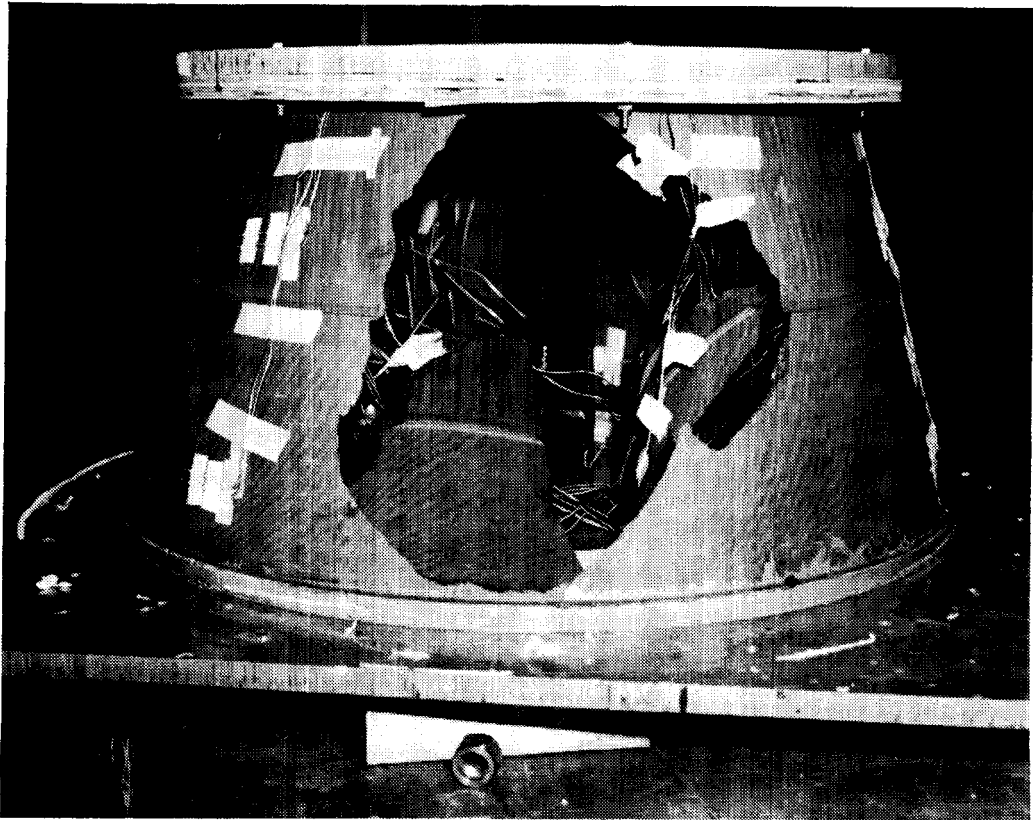


Figure 5. Failed cone.

E. Test Results

Figure 6 plots circumferential strain recorded by the uniaxial gages against applied air pressure. All strains increased with increased applied pressure. This response was expected.

Since the axial load due to water pressure above the cone was carried by the metal bridge, the axial strains should be small. Figures 7 to 12 plot axial strain recorded by the inside and outside biaxial gages against applied pressure. The inside strains were low and were as expected at all applied pressures. The resulting axial strains were due to the meridional component of the water pressure and to meridional cone bending. The outside gages, however, measured high strains at low applied pressures. This may be due to an increase in the resistance at the outside gage locations. A silicon water proofer applied to all outside gages, the plastic sheathing encompassing the cone exterior, and/or moisture are three possible causes of the increased resistance. The affects of these three possible causes as well as other test parameters on the resistance will be studied by the Materials Laboratory at MSFC by subsequent strain gage testing.

Figures 13 to 21 plot circumferential strain recorded by the inside and outside biaxial gages against applied pressure. The inside gages measured increasing strain with increasing applied pressure. This, again, is the expected response due to the applied loading. The outside gages measured high strains at low applied pressures and, again, this is probably due to an increased resistance.

PARD CCT1 NOZZLE BUCKLING TEST RESULTS
 MSFC STRUCTURE AND PROPULSION LAB EP48

U4 UNIAxIAL GAGE AT 270 DEGRS.
 U3 UNIAxIAL GAGE AT 180 DEGRS.
 U2 UNIAxIAL GAGE AT 90 DEGRS.
 U1 UNIAxIAL GAGES AT 0 DEGRS.

◆ U4
 □ U3
 △ U2
 X U1

DATE: 03/25/88
 TIME: 13139:23

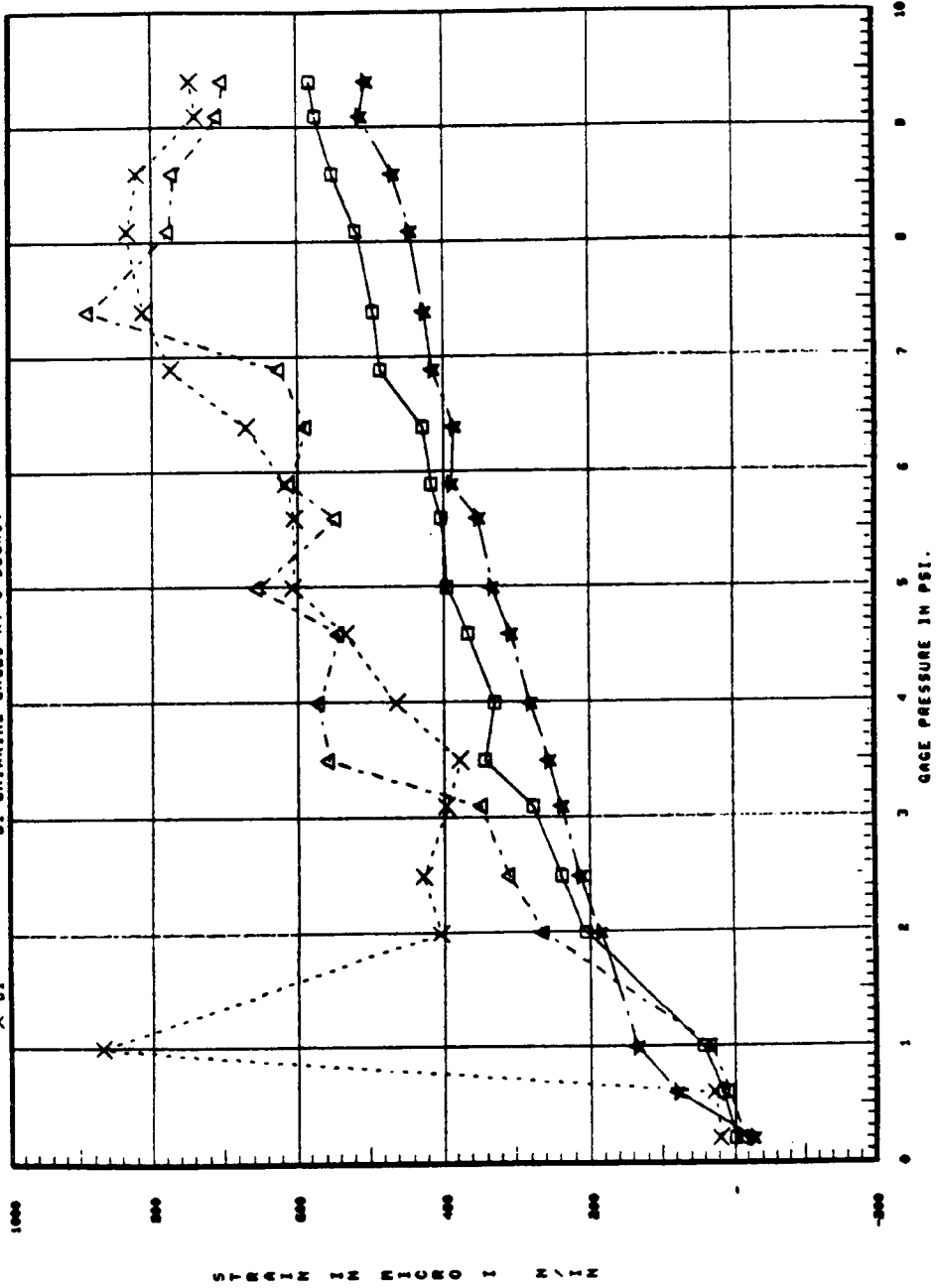


Figure 6. Circumferential strains recorded by uniaxial gages plotted against applied pressure.

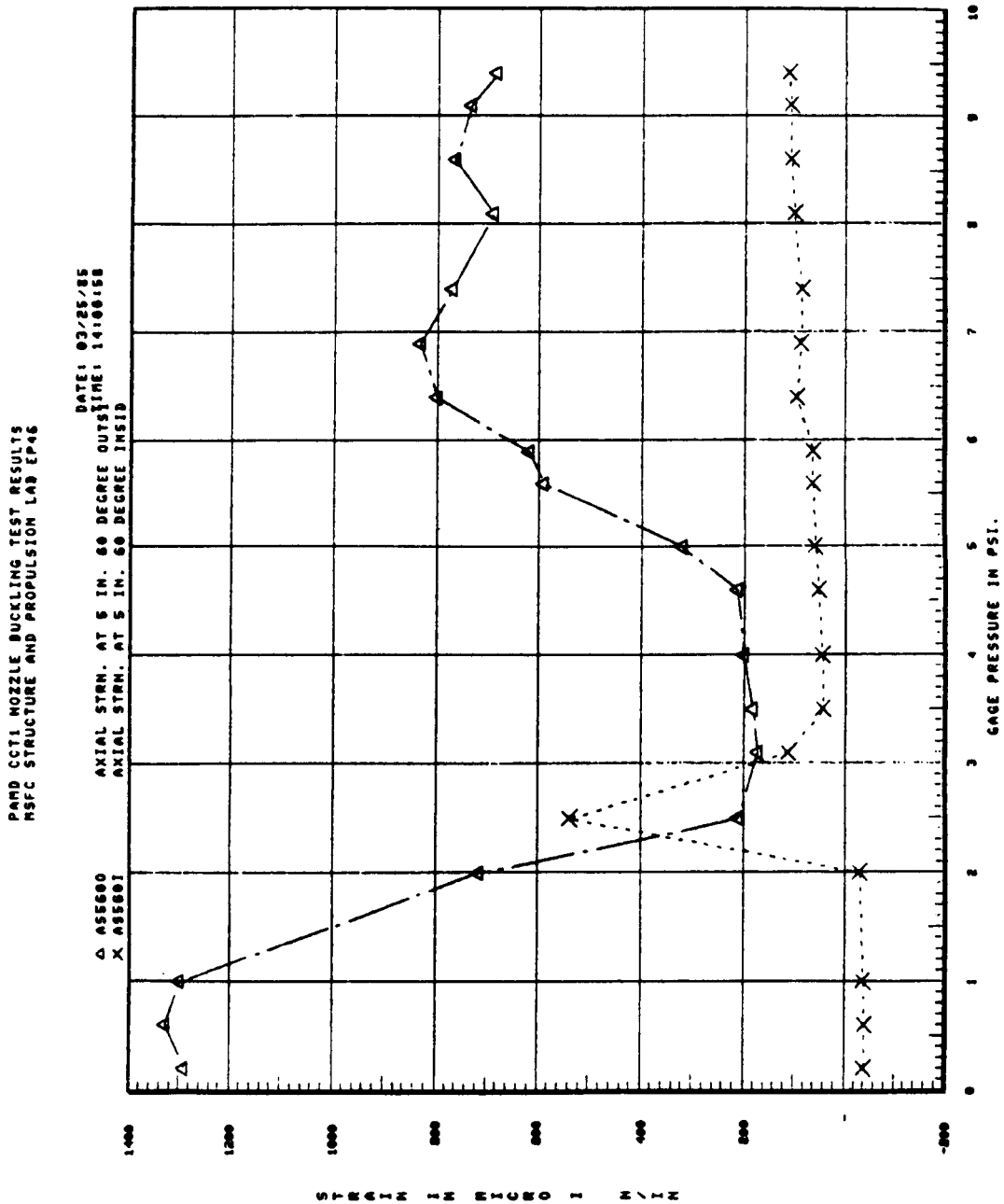


Figure 7. Inside/outside axial strain at 5-3/8 in. and 60 deg plotted against applied pressure.

PAND CCT1 NOZZLE BUCKLING TEST RESULTS
 NSFC STRUCTURE AND PROPULSION LAB EP46

DATE: 03/25/85
 TIME: 141021Z

△ ASS1000 AXIAL STRN. AT 5 IN. 180 DEGREE OUTSIDE
 X ASS1001 AXIAL STRN. AT 5 IN. 180 DEGREE INSIDE

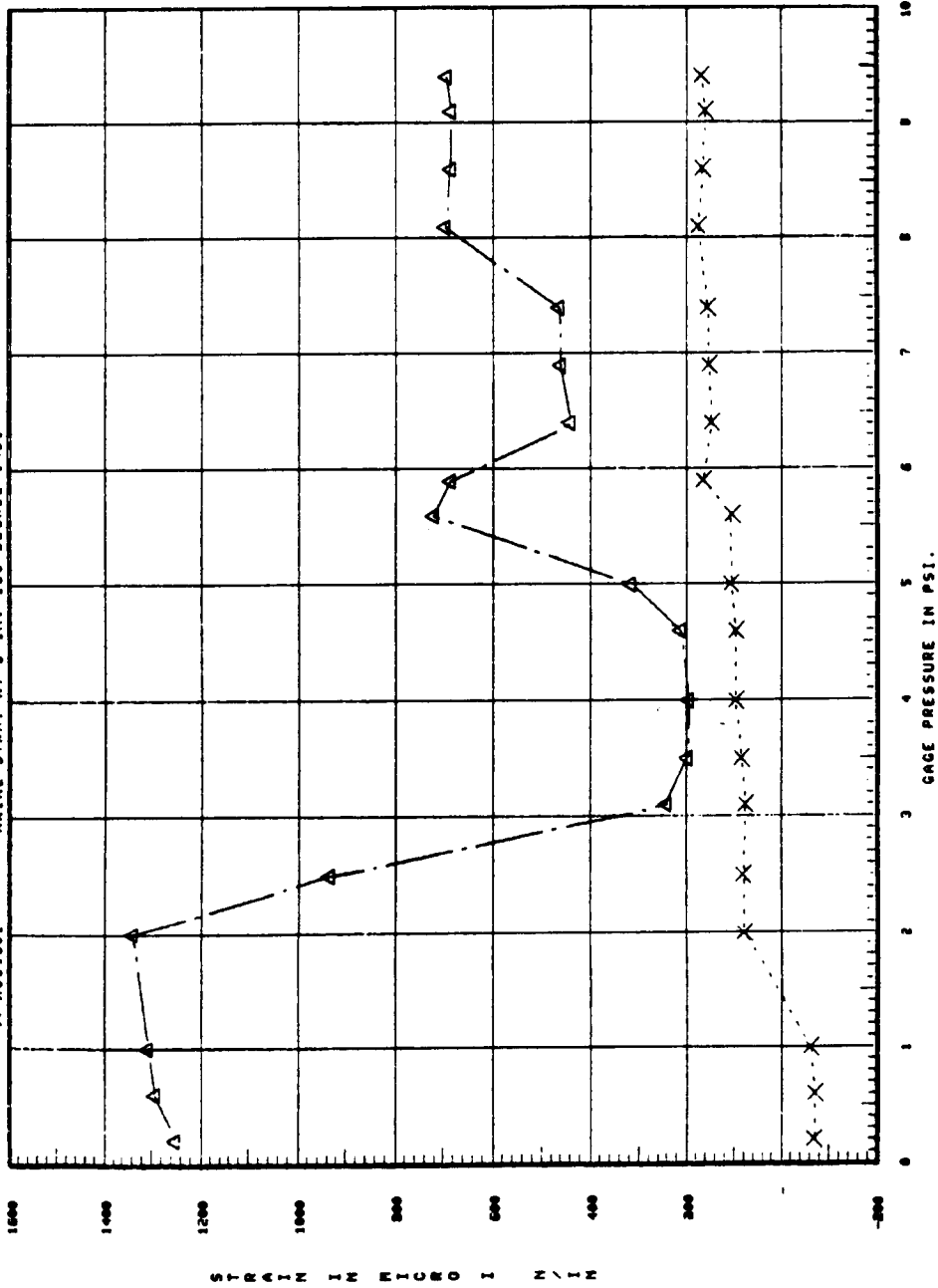


Figure 8. Inside/outside axial strain at 5-3/8 in. and 180 deg plotted against applied pressure.

PARD CCT1 NOZZLE BUCKLING TEST RESULTS
 MSFC STRUCTURE AND PROPULSION LAB EP46

DATE: 03/25/85
 OUTSIDE AXIAL STRAIN AT 5 IN. 300 DEGREE
 INSIDE AXIAL STRAIN AT 5 IN. 300 DEGREE

△ ASS3000
 X ASS3001

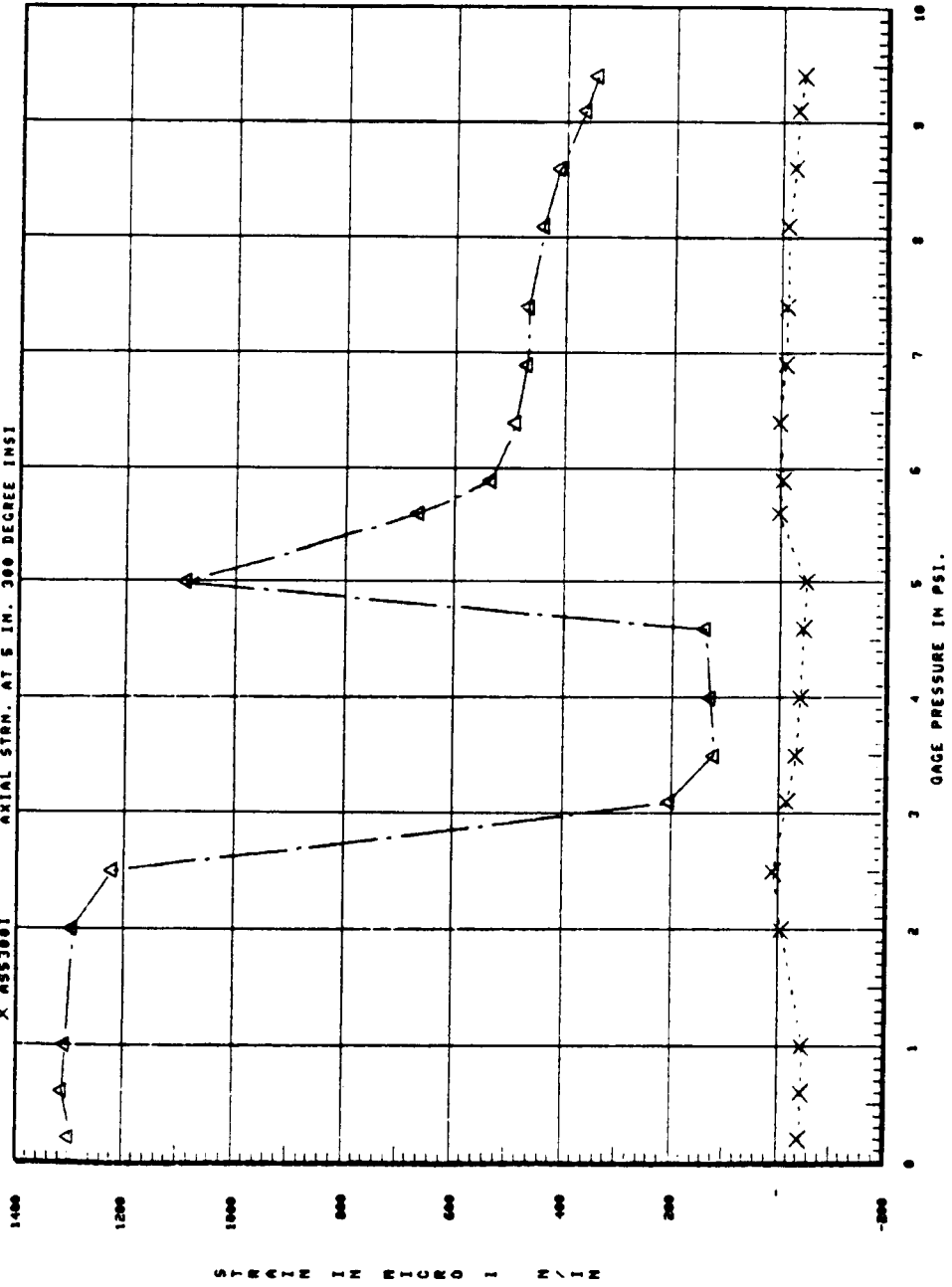


Figure 9. Inside/outside axial strain at 5-3/8 in. and 300 deg plotted against applied pressure.

ORIGINAL PAGE IS
OF POOR QUALITY

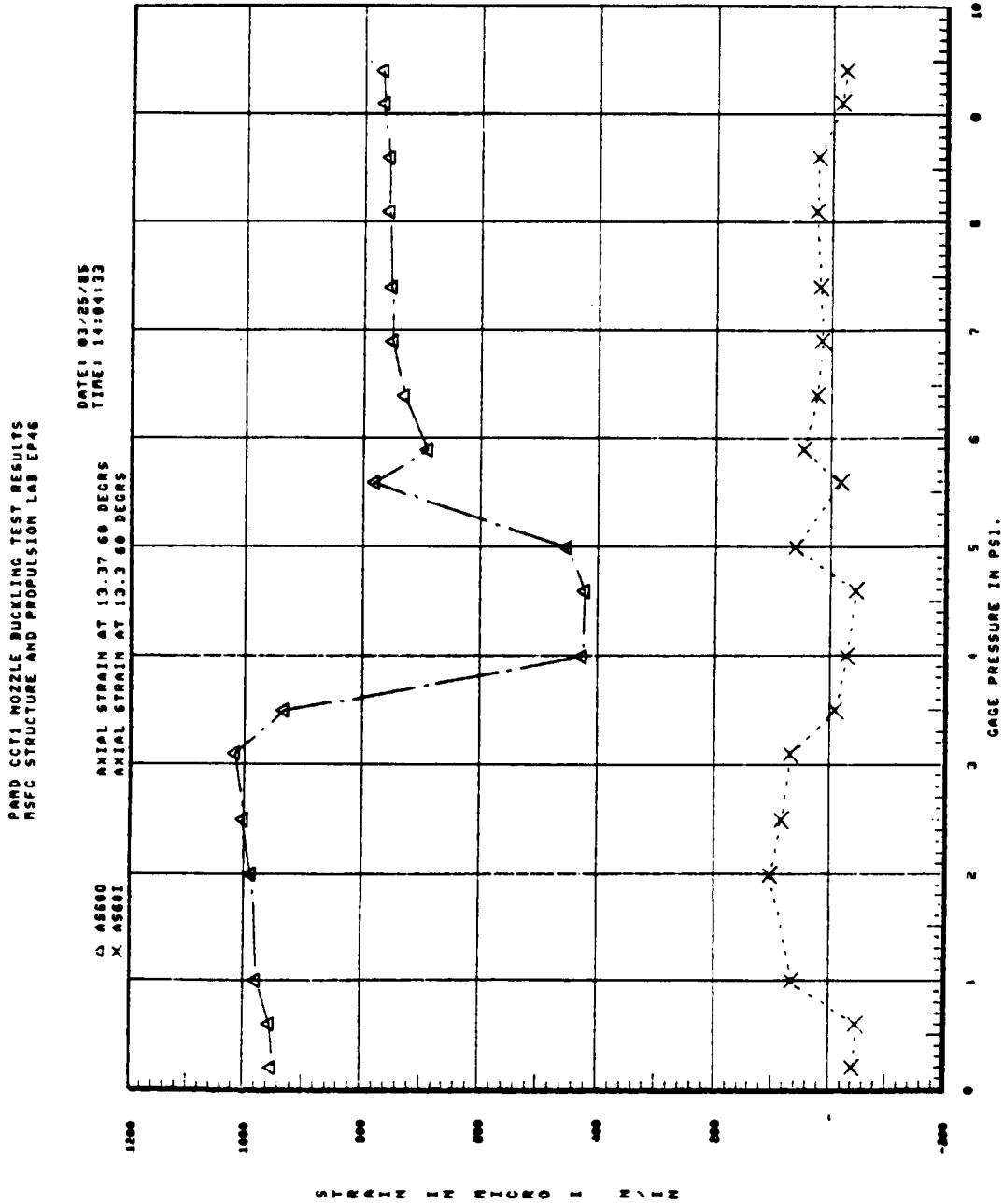


Figure 10. Inside/outside axial strain at 13-1/8 in. and 60 deg plotted against applied pressure.

PARD CCT1 NOZZLE BUCKLING TEST RESULTS
 NSFC STRUCTURE AND PROPULSION LAB EP46

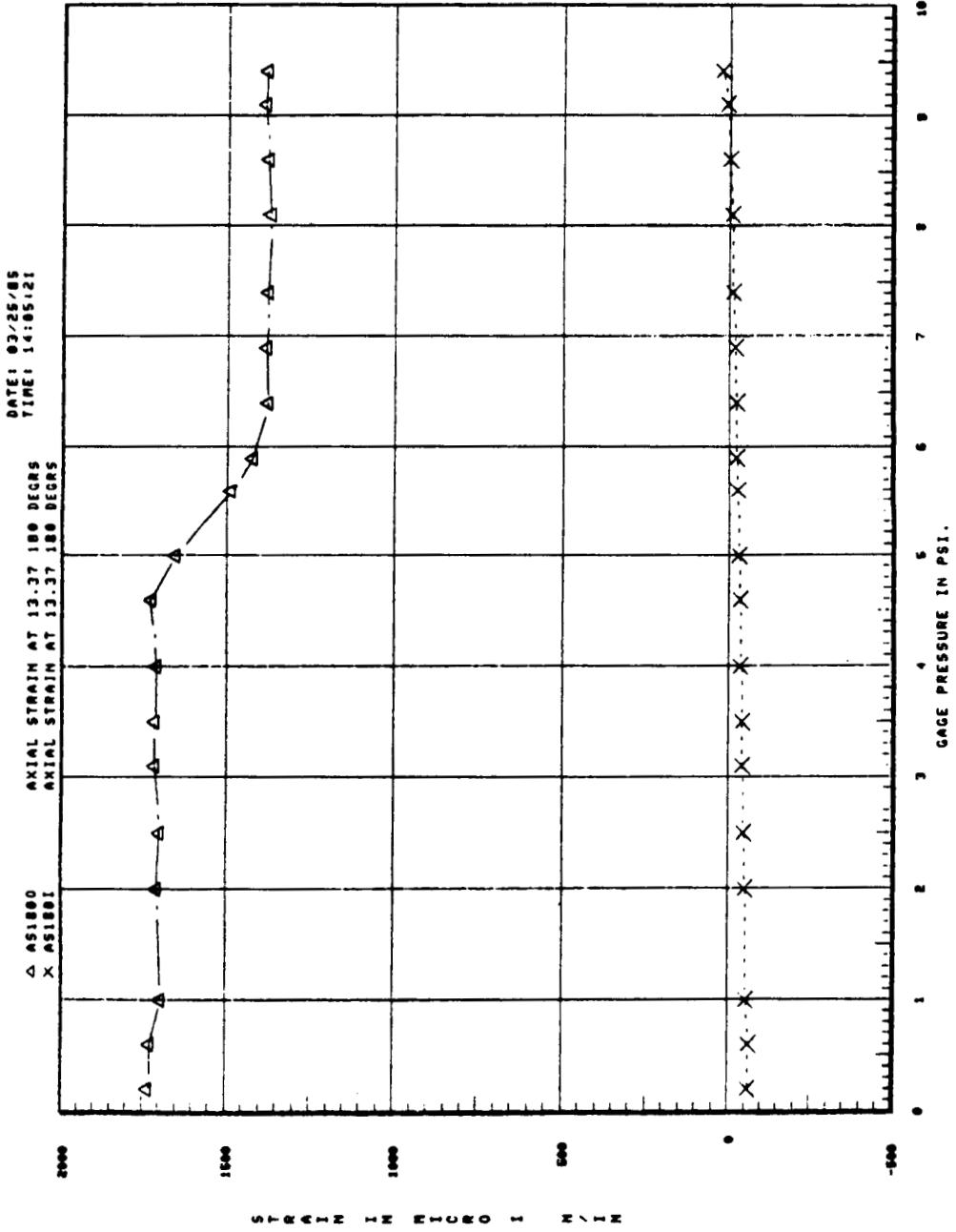


Figure 11. Inside/outside axial strain at 13-1/8 in. and 180 deg plotted against applied pressure.

ORIGINAL PAGE IS
OF POOR QUALITY

PARD CCT1 NOZZLE BUCKLING TEST RESULTS
NSFC STRUCTURE AND PROPULSION LAB EP4E

DATE: 03/25/85
TIME: 14106:25

AXIAL STRAIN AT 13.37 300 DEGRS
AXIAL STRAIN AT 13.37 300 DEGRS

△ AS3000
X AS3001

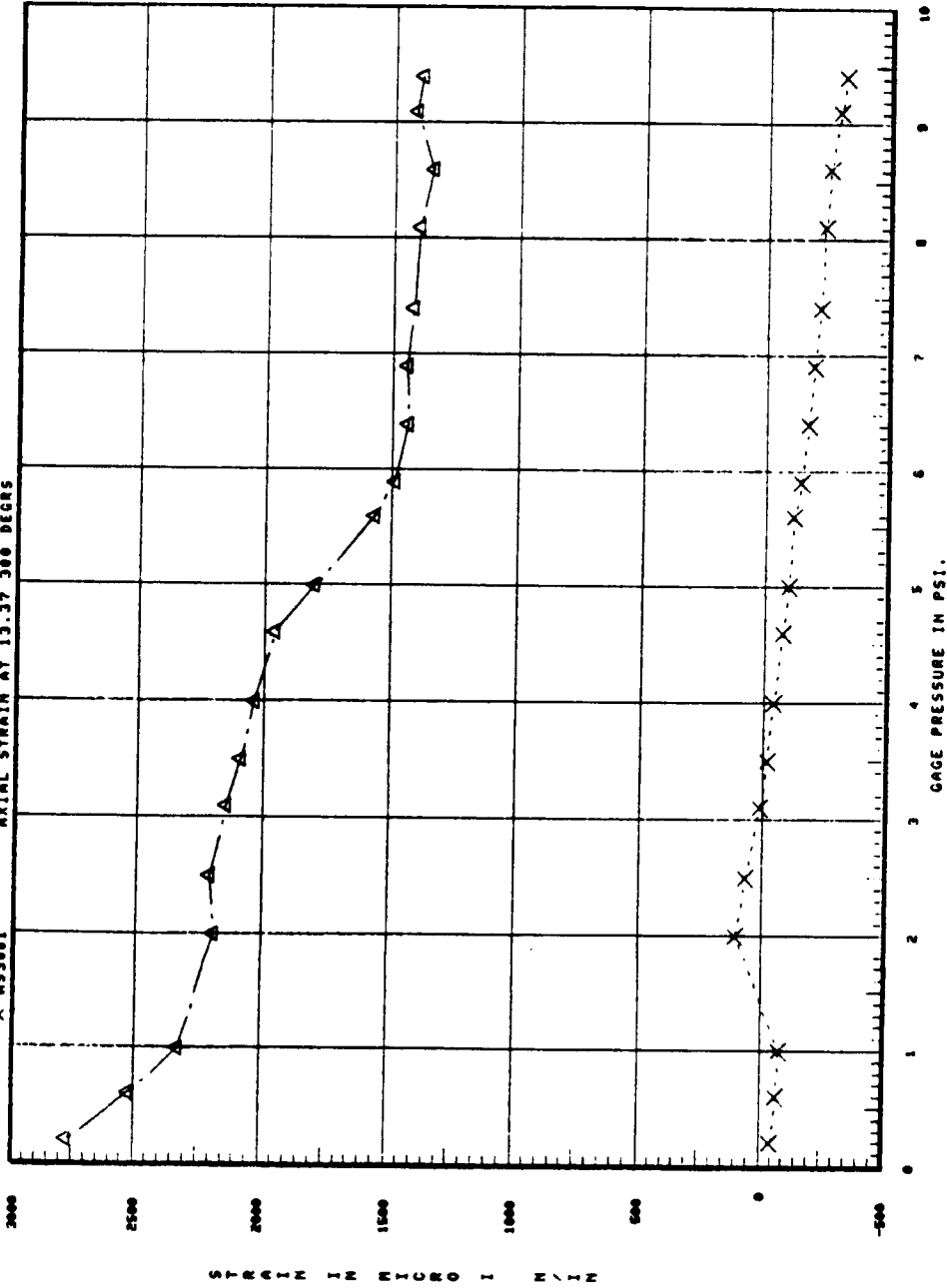


Figure 12. Inside/outside axial strain at 13-1/8 in. and 300 deg plotted against applied pressure.

PARD CCT1 NOZZLE BUCKLING TEST RESULTS
 MSFC STRUCTURE AND PROPULSION LAB EP46

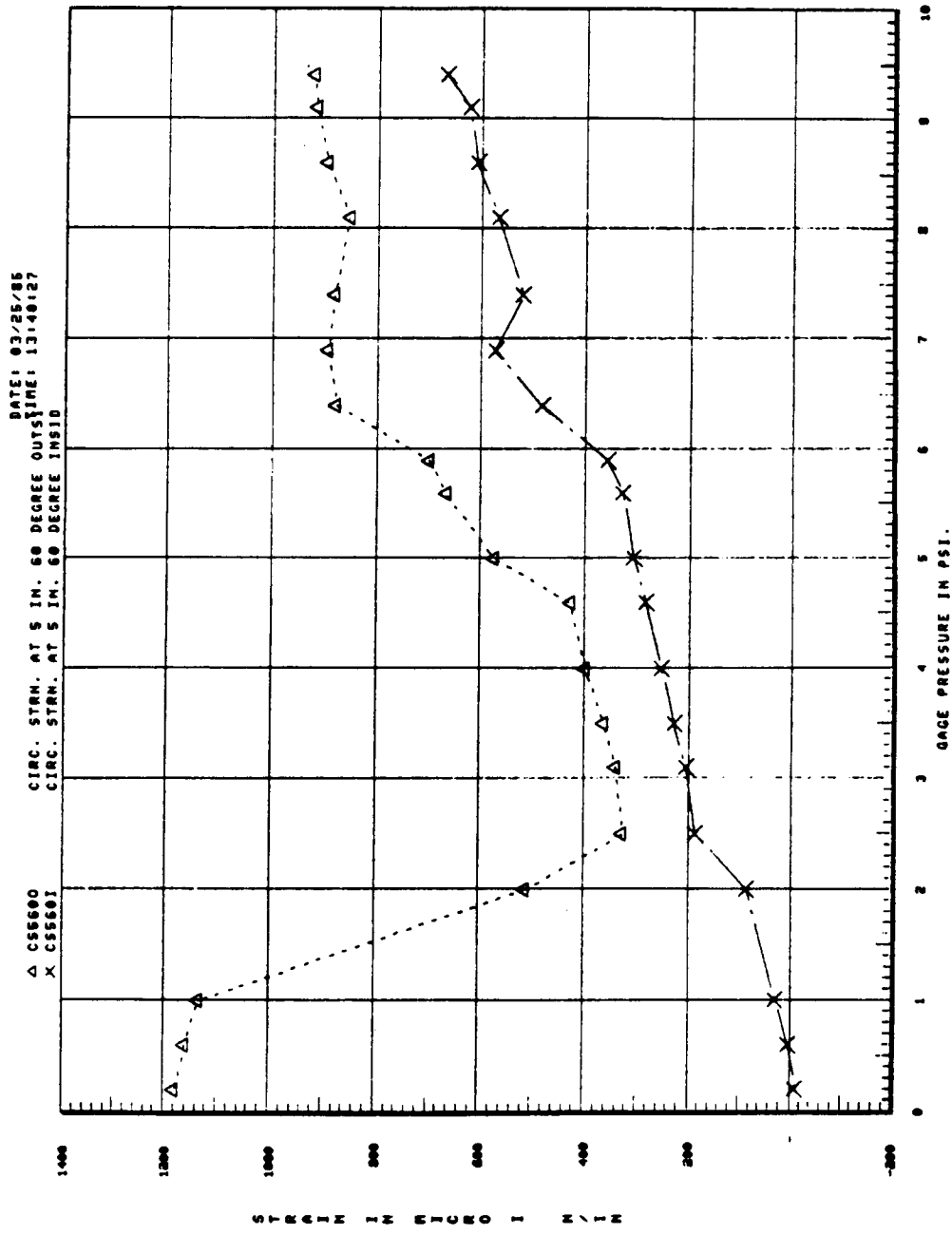


Figure 13. Inside/outside circumferential strain at 5-3/8 in. and 60 deg plotted against applied pressure.

ORIGINAL PAGE IS
OF POOR QUALITY

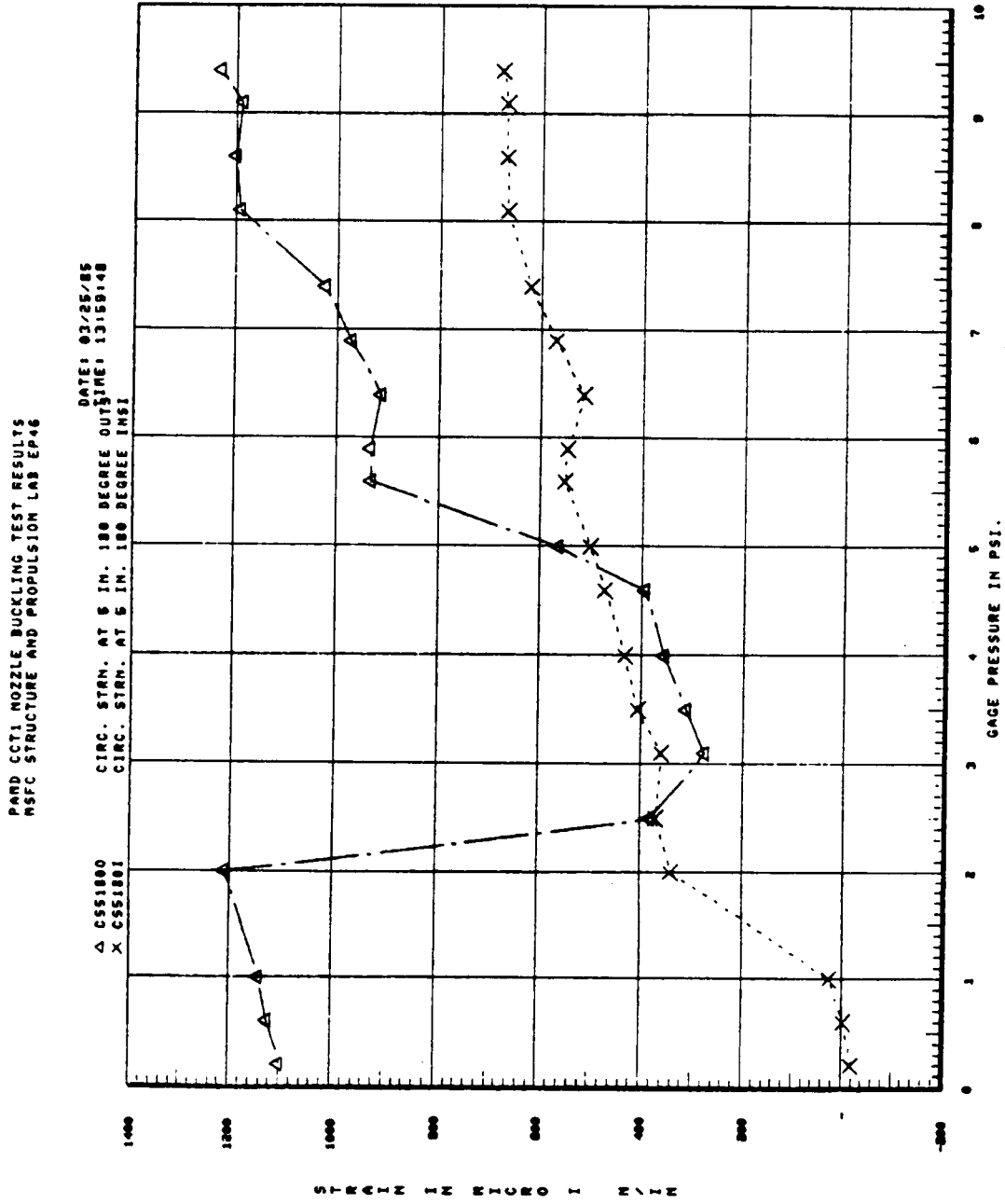


Figure 14. Inside/outside circumferential strain at 5-3/8 in. and 180 deg plotted against applied pressure.

PAMP CCT1 NOZZLE BUCKLING TEST RESULTS
NSFC STRUCTURE AND PROPULSION LAB EP46

DATE: 03/25/85
CIRC. STRN. AT 5 IN. 300 DEGREE OUTSIDE
CIRC. STRN. AT 5 IN. 300 INSIDE

△ C553000
X C553001

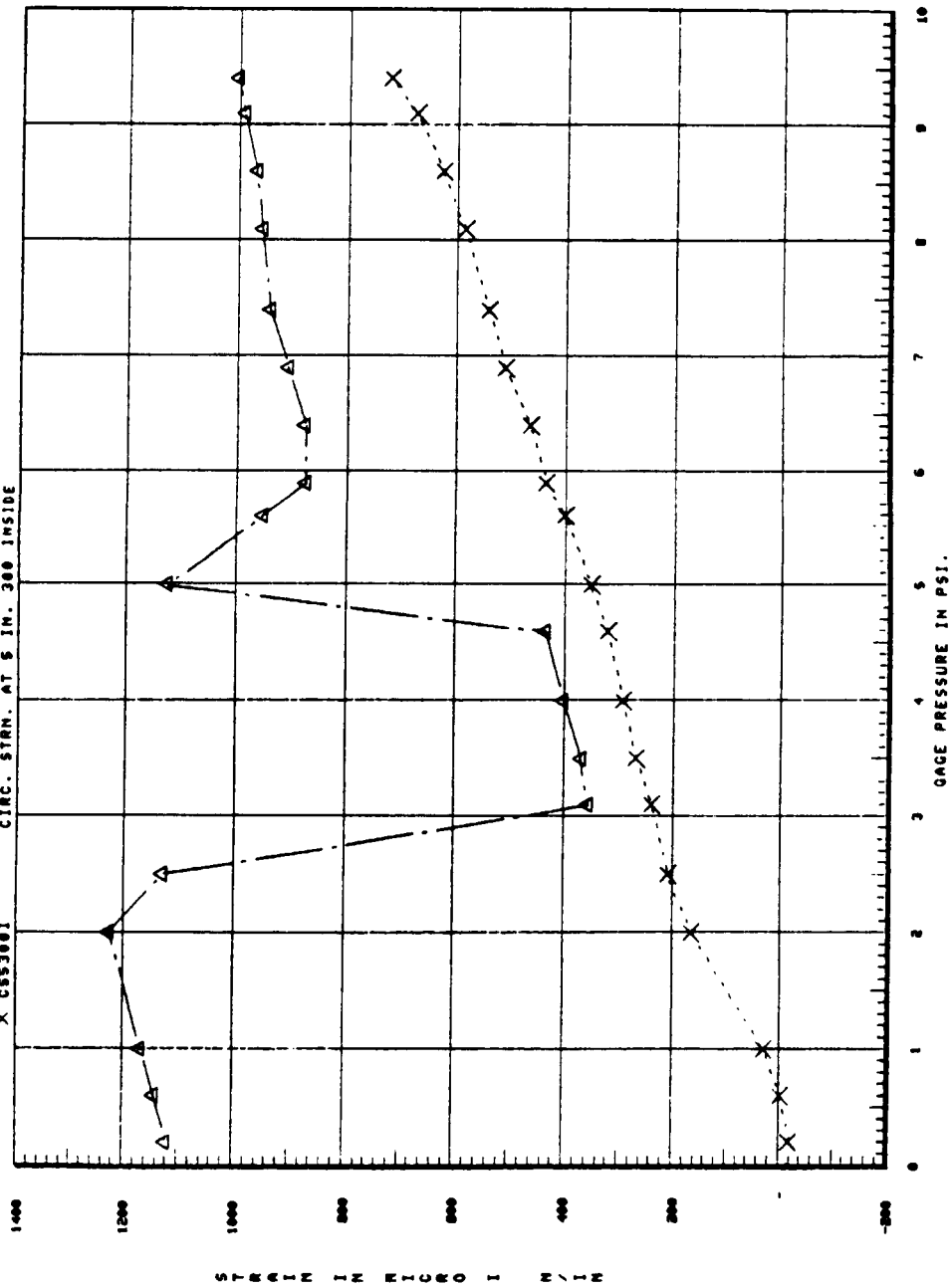


Figure 15. Inside/outside circumferential strain at 5-3/8 in. and 300 deg plotted against applied pressure.

ORIGINAL PAGE IS
OF POOR QUALITY

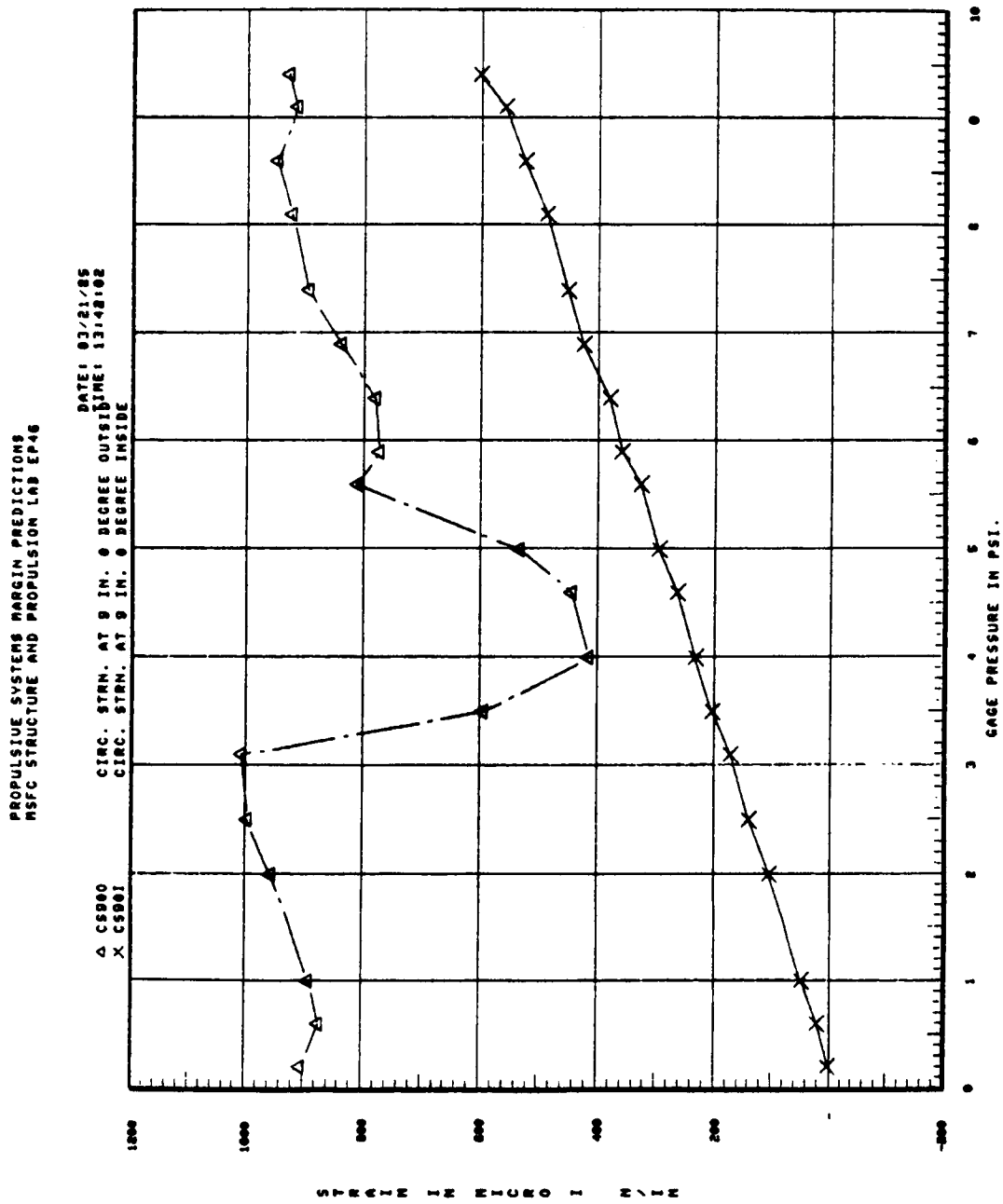


Figure 16. Inside/outside circumferential strain at 9-7/8 in. and 0 deg plotted against applied pressure.

PROPULSIVE SYSTEMS MARGIN PREDICTIONS
 NSFC STRUCTURE AND PROPULSION LAB EP-46

DATE: 03/21/85
 CIRC. STRN. AT 9 IN. 120 DEGREE OUTSIDE: 13147108
 CIRC. STRN. AT 9 IN. 120 DEGREE INSI

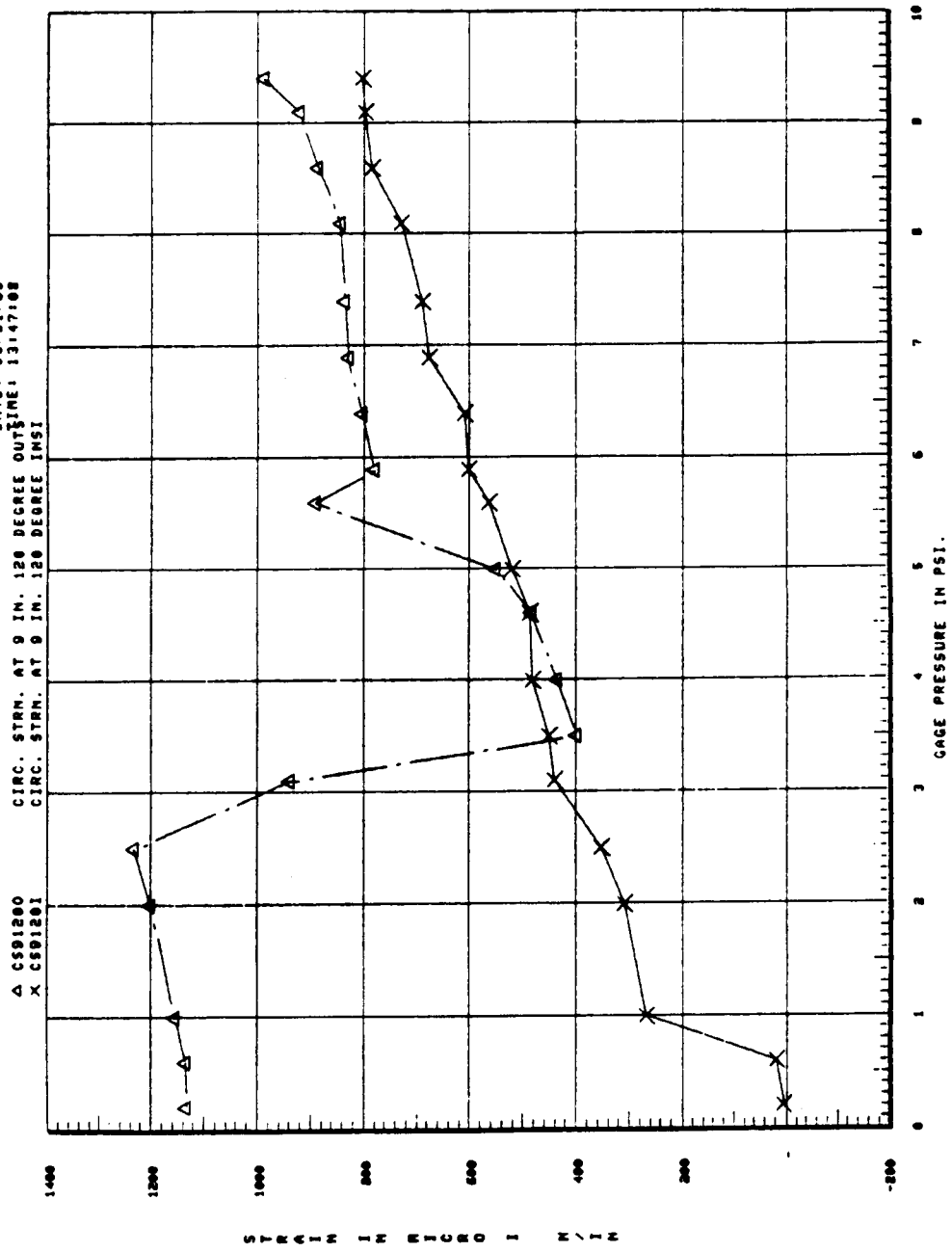


Figure 17. Inside/outside circumferential strain at 9-7/8 in. and 120 deg plotted against applied pressure.

PROPULSIVE SYSTEMS MARGIN PREDICTIONS
 MSFC STRUCTURE AND PROPULSION LAB EP46

DATE: 03/21/85
 TIME: 13:48:03

△ CS92400
 X CS92401

CIRC. STRN. AT 9 IN. 240 DEGREE OUTSIDE
 CIRC. STRN. AT 9 IN. 240 DEGREE INSIDE

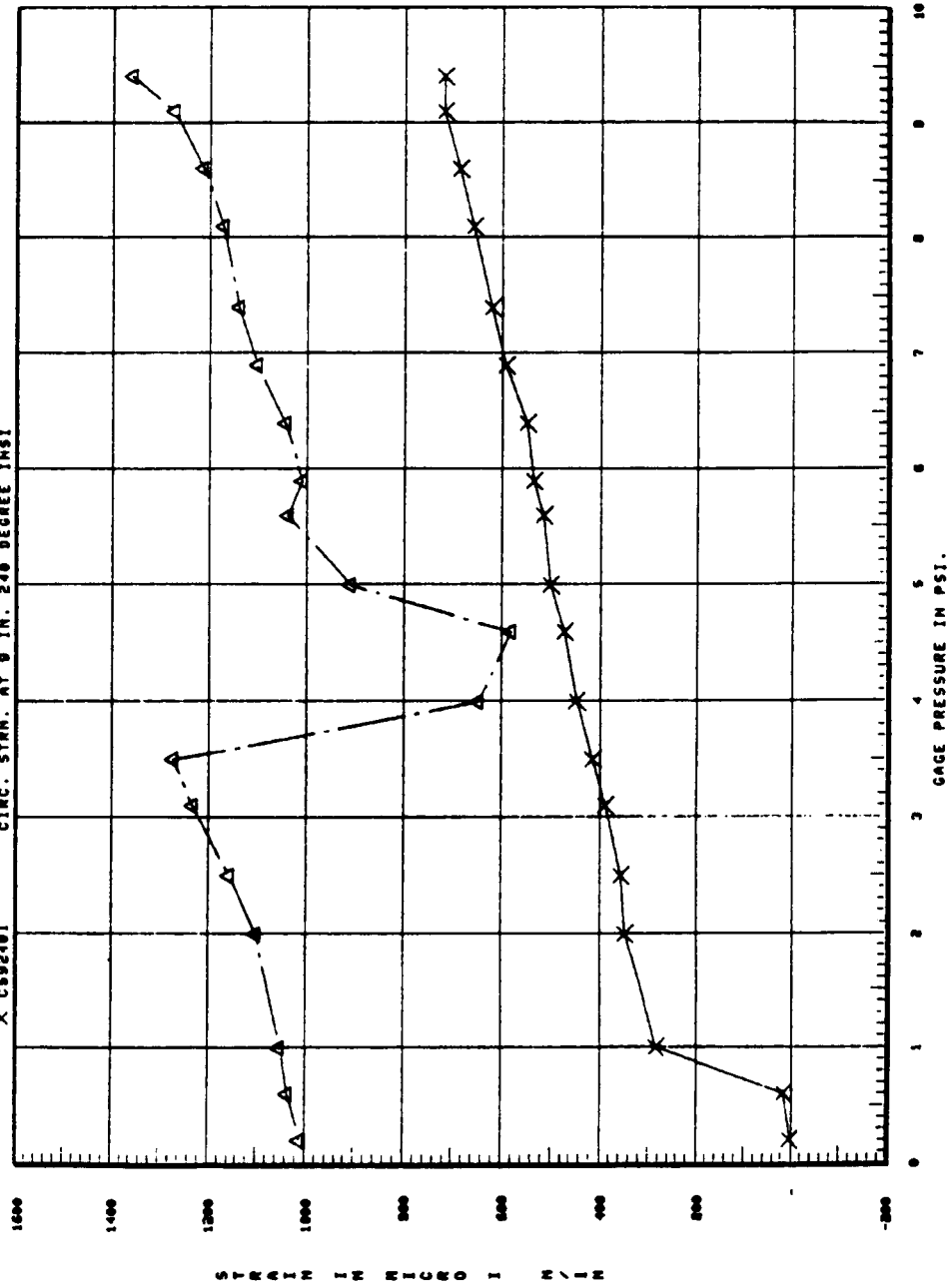


Figure 18. Inside/outside circumferential strain at 9-7/8 in. and 240 deg plotted against applied pressure.

PARD CCT1 NOZZLE BUCKLING TEST RESULTS
 MSC STRUCTURE AND PROPULSION LAB EP46

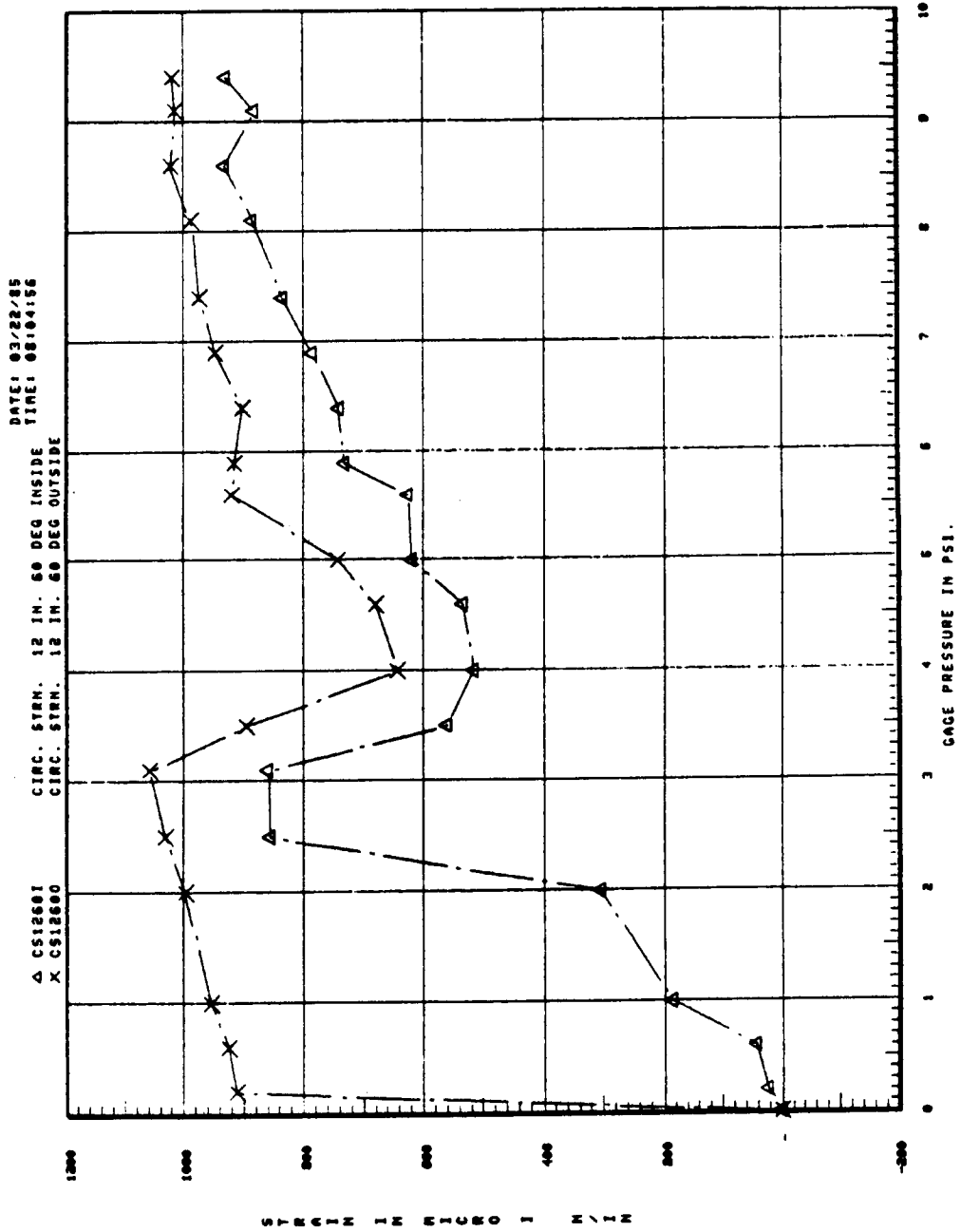


Figure 19. Inside/outside circumferential strain at 13-1/8 in. and 60 deg plotted against applied pressure.

PARD COTL NOZZLE BUCKLING TEST RESULTS
 NSFC STRUCTURE AND PROPULSION LAB EP46

DATE: 03/22/85
 CIRC. STRN. 12 IN. 180 DEG OUTSIDE TIME: 08106102
 CIRC. STRN. 12 IN. 180 DEG INSIDE

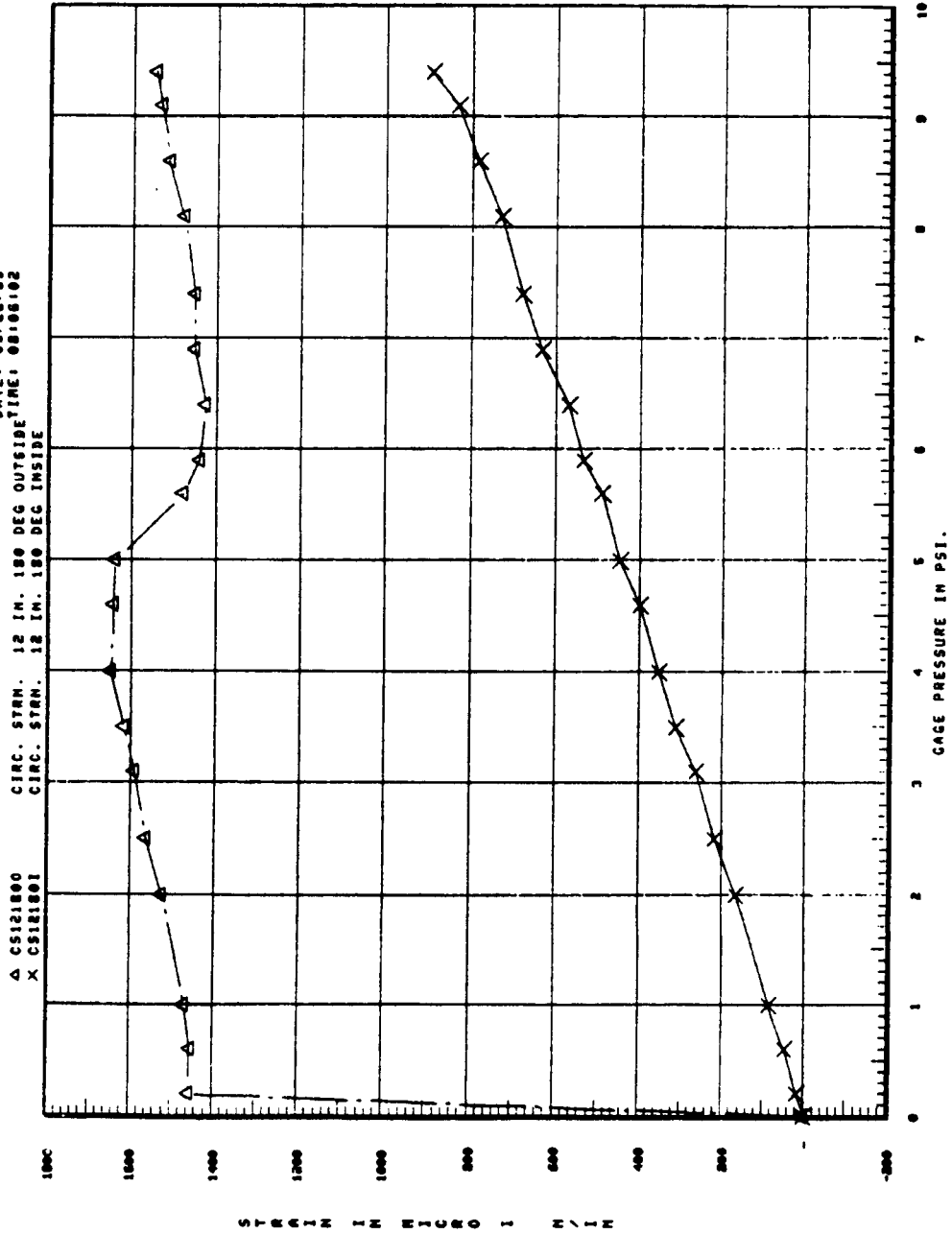


Figure 20. Inside/outside circumferential strain at 13-1/8 in. and 180 deg plotted against applied pressure.

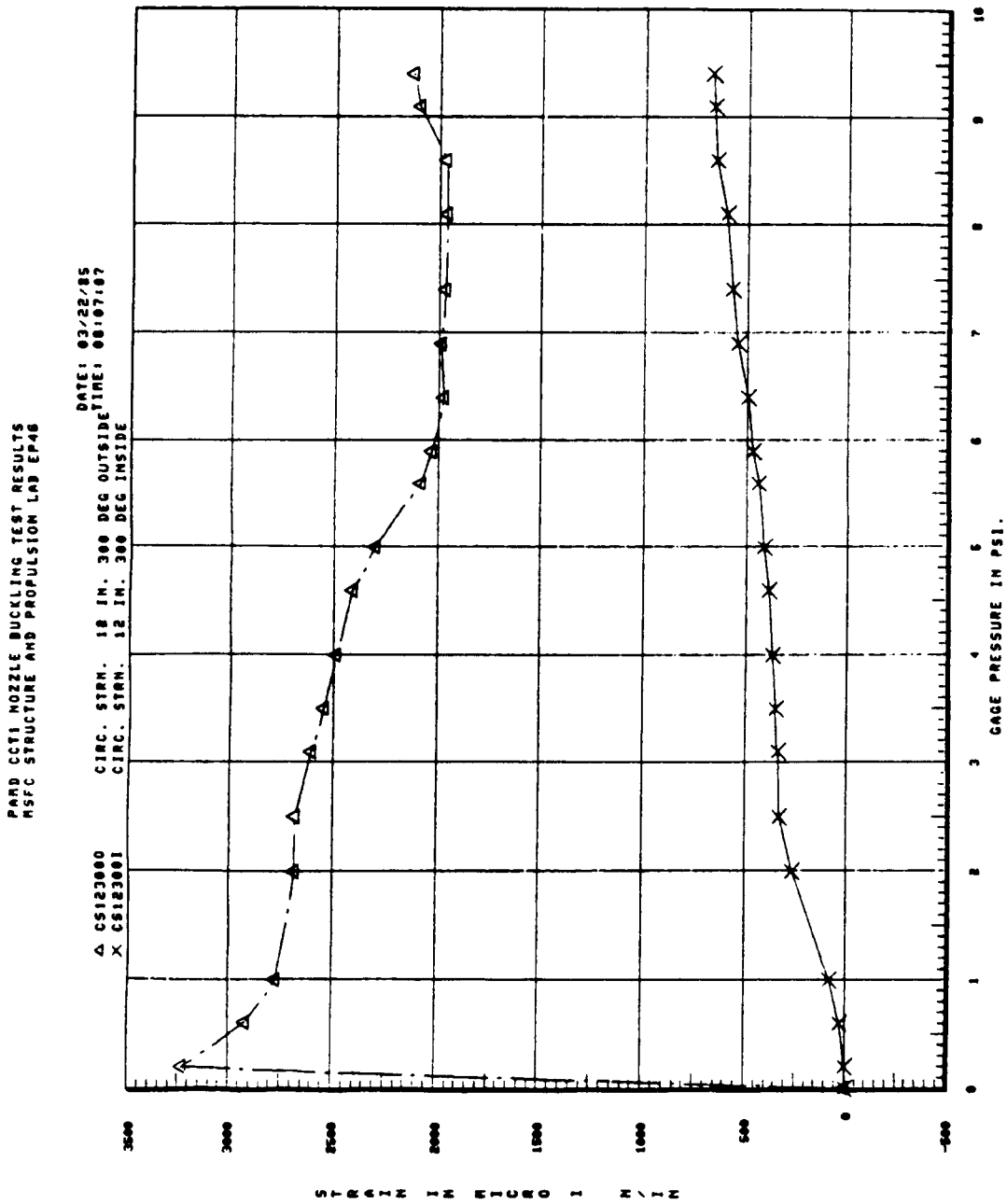


Figure 21. Inside/outside circumferential strain at 13-1/8 in. and 300 deg plotted against applied pressure.

III. SPAR FINITE ELEMENT MODEL

A bifurcation buckling solution was performed using the SPAR finite element code. The SPAR model of the test specimen was constructed with rectangular shell elements, E43. These elements have bending and membrane stiffness capabilities. Figure 22 shows one view of the constructed model.

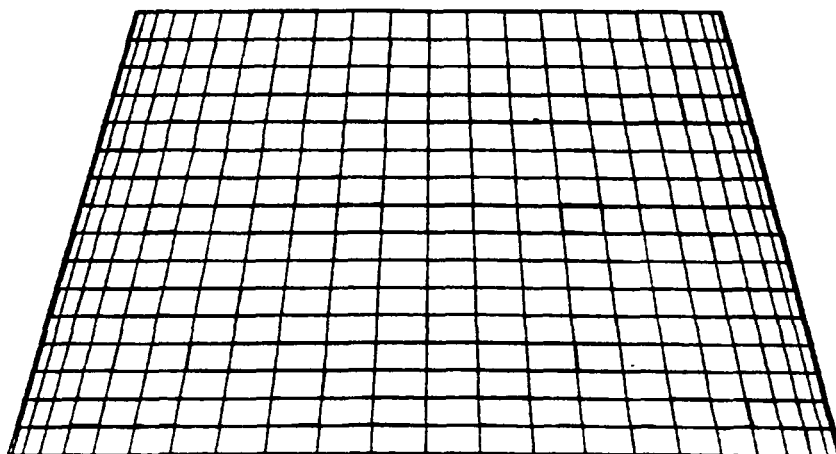


Figure 22. Constructed SPAR model.

The carbon-carbon cone is a fiber-reinforced composite with anisotropic material properties. However, inputting anisotropic material properties for rectangular shell elements is difficult with the current version of SPAR, so an isotropic solution was performed as an approximation. The model material properties were approximated by an "equivalent" isotropic modulus of elasticity. The "equivalent" modulus was calculated by scaling the modulus of elasticity in the axial and hoop directions according to the equation for the buckling pressure of an orthotropic cone [equation (1)]

$$P_{cr} = \frac{0.86 \gamma}{(1 - \mu_{\theta}\mu_z)^{3/4}} E_{\theta}^{0.75} E_z^{0.25} \left(\frac{P}{L}\right) \left(\frac{t}{P}\right)^{5/2} \quad (1)$$

so that

$$E_{equ} = E_{\theta}^{0.75} E_z^{0.25}$$

Material properties for the aft end of the cone were not available. However, material properties for the forward end of the cone in the axial and hoop directions at room temperature were provided by Prototype Development Associates (PDA). The "equivalent" isotropic modulus was calculated to be 1.48×10^6 psi using the properties available at the forward end.

Nodal rows that correspond to the top and base of the cone (first and last nodal rows) were constrained by the SPAR code, so that all six degrees of freedom at these nodes are zero. This simulated the fixed-fixed boundary condition of the test configuration.

The added stiffness due to the stiffening ring was approximated in the model by increasing the thickness of one row of elements at a location which corresponds to the stiffening ring location. This resulted in equivalent moments of inertia at the stiffening ring location for both the cone and the cone model.

Model pressure loading was separated into two load components. The first component simulated the head pressure by a linear pressure profile that varied from 0.35 psi at the top to 0.9 psi at the base. The second load component simulated the applied air pressure by a constant unit pressure profile of 1.0 psi. Since the head pressure was constant for the duration of the test, the first load component was applied to the model as a preload. Then a bifurcation buckling solution of the form $A\nu = \lambda B\nu$ was performed with the second load component. This loading scheme simulated the actual loading of the test specimen in the test fixture. Figure 23 illustrates the model pressure profiles.

SPAR predicted a critical applied pressure of 8.76 psi. Therefore, the critical total pressure is a linear pressure profile varying from 9.11 psi (0.35 + 8.76) at the top to 9.66 psi (0.9 + 8.76) at the base, due to head plus applied pressure. Figure 24 illustrates the critical pressure loading. Figures 25 and 26 show two views of the buckling mode predicted by SPAR.

Stresses induced by the total critical pressure were calculated by a SPAR stress run. Calculated element stresses, which correspond to strain gage locations, are listed in Table 2.

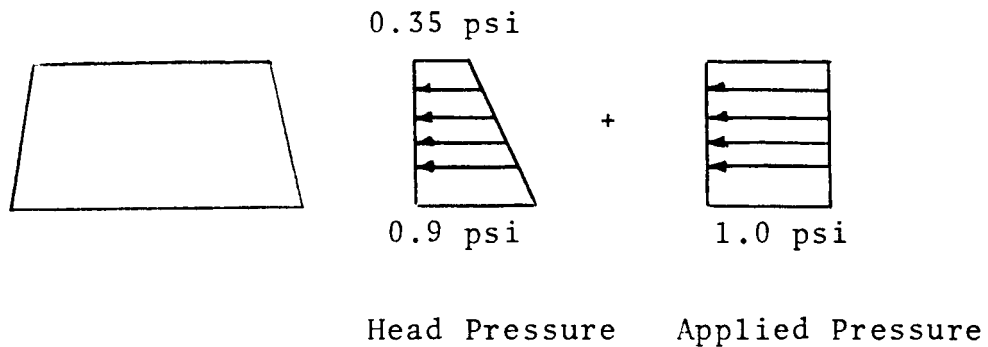


Figure 23. SPAR model applied loading.

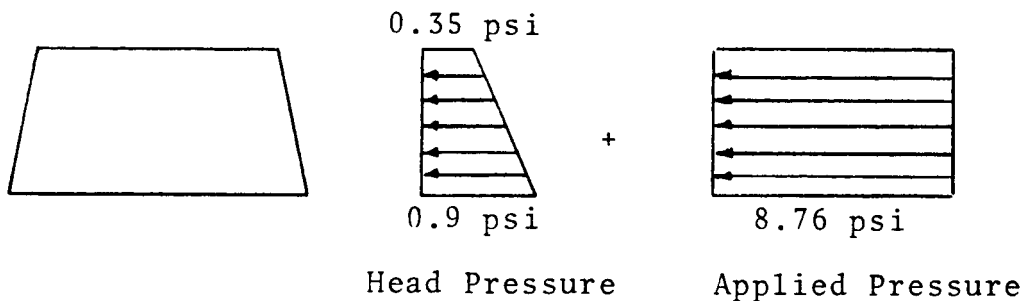


Figure 24. Analytical buckling load.

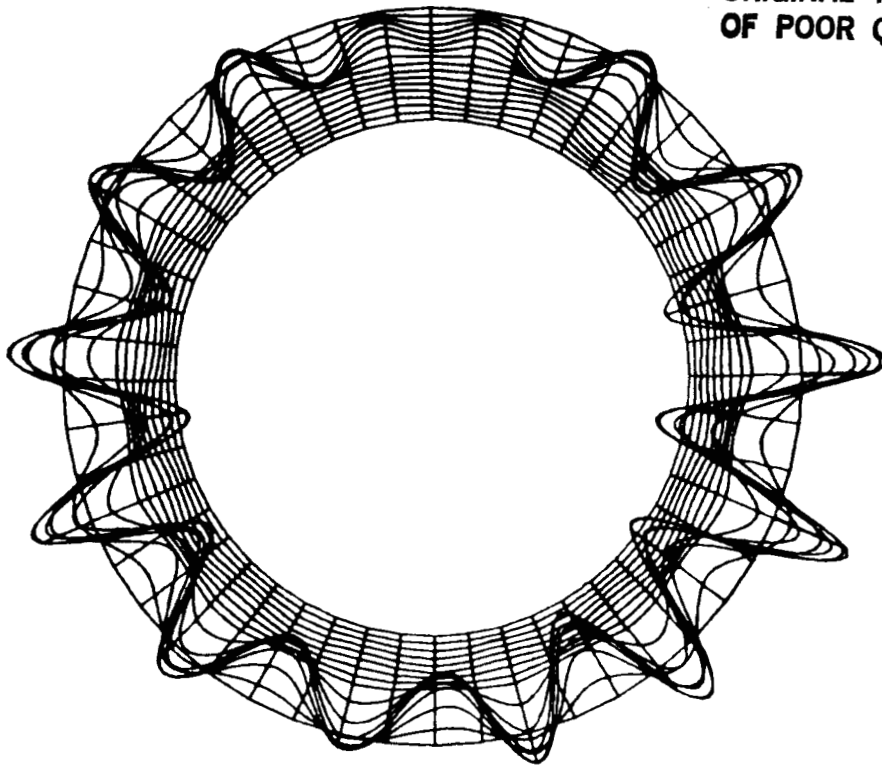


Figure 25. Predicted buckling mode (axial view).

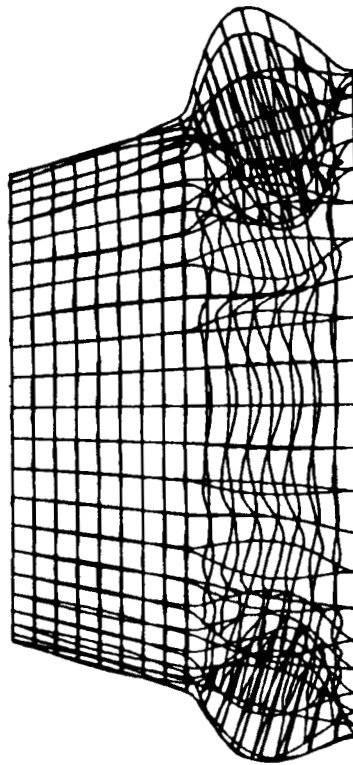


Figure 26. Predicted buckling mode (side view).

TABLE 2. CIRCUMFERENTIAL AND AXIAL ELEMENT STRESSES DUE TO THE CRITICAL APPLIED PRESSURE (8.76 psi)

Cone Height (in.)	Stress (psi)
Circumferential:	
5-3/8	-1307.75
9-7/8	-1466.2
13-1/8	-1821.03
Axial:	
5-3/8	213.9
9-7/8	-141.18
13-1/8	-55.6

IV. DISCUSSION

This section compares the measured and predicted buckling pressures and calculates the material correlation factor. Also, comparisons are made between the measured and predicted circumferential strains at various cone locations.

The material correlation factor is $(9.75/8.76) = 1.1$. This shows a good correlation between the model and the test specimen, since the correlation factor is near unity. However, material defects weaken the structure, so, theoretically, the correlation factor should be less than unity.

The correlation factor exceeds unity because the model stiffness, which was approximated using equation (1), was underpredicted. Also, equation (1) neglects the radial stiffness contribution, E_r . An anisotropic solution, which is easily performed with other finite elements codes, would be a more accurate solution and would result in a stiffer model.

An underpredicted model stiffness may also be attributed to the available global material properties (E_θ , E_z , E_r). Material properties for only the forward portion of the exit cone were available; however, the hydroburst test was conducted on the aft portion of the cone. This discrepancy may contribute to the low model stiffness.

Measured and predicted circumferential strains at various inside locations are compared in Table 3 to further evaluate model accuracy. Inside gages were used for the comparison, since outside gages were affected by a resistance increase. Measured circumferential strains at a specific height and pressure loading varied with circumferential location. For example, in Table 3, the circumferential strain at 12-7/8 in. for a 9.5 psi applied pressure varied from 650×10^{-6} in./in. at 300 deg to 920×10^{-6} in./in. at 60 deg. For elastic buckling, all strains at a specific cone height should be identical since the hydrostatic pressure is symmetrical about the cone centerline. Since there is no evidence that the cone buckled plastically, the strain variation is unwarranted and undesirable. This strain variation may be a characteristic of carbon-carbon involutes subjected to hoop stress and is presently being examined by the Materials and Processes Laboratory at MSFC.

TABLE 3. MEASURED AND PREDICTED CIRCUMFERENTIAL STRAIN COMPARISON AT VARIOUS CONE LOCATIONS

Measured Circumferential Strain due to 9.5 psi (10^{-6} in./in.)						
<u>Cone Height</u>	<u>0°</u>	<u>60°</u>	<u>120°</u>	<u>180°</u>	<u>240°</u>	<u>300°</u>
5-3/8		-670		-680		-720
9-7/8	-600		-800		-720	
13-1/8		-920		-880		-650
Measured Circumferential Strain Averaged and Compared to the Corresponding Predicted Strain ($\times 10^{-6}$ in./in.)						
<u>Cone Height</u>	<u>Measured</u>	<u>Predicted</u>	<u>Correlation Factor</u>			
5-3/8	-690	-883.6	0.78			
9-7/8	-707	-990.6	0.71			
13-1/8	-817	-1230.4	0.66			

In order to account for the strain variation, so that the measured and predicted stresses can be compared, the measured circumferential strains at each cone height were averaged. The average strains are then compared to the corresponding predicted strains in Table 3 and a correlation factor based on strain was calculated. Predicted strains are considerably higher than the measured strains at all three cone heights. Again, this is due to an underpredicted material modulus.

V. CONCLUSIONS


The SPAR model proved to be an accurate test for predicting the buckling pressure of the test cone. The correlation factor was calculated to be 1.1. This provides confidence in the SPAR modeling technique which will be used to evaluate CCT-2.

The modulus of elasticity, which was approximated for an isotropic solution, was underpredicted in the model. This resulted in predicted strains which were higher than the measured and a predicted buckling pressure which was lower than the measured. Adjusting the isotropic modulus or performing a more exact anisotropic solution would produce a more accurate model.

Finally, it should be noted that this is only one test. Subsequent tests should be performed to account for drift.

REFERENCES

1. Buckling of Thin-Walled Truncated Cones. NASA Space Vehicle Design Criteria, NASA, September 1968.

1. REPORT NO. NASA TP-2556		2. GOVERNMENT ACCESSION NO.		3. RECIPIENT'S CATALOG NO.	
4. TITLE AND SUBTITLE Hydroburst Test of a Carbon-Carbon Involute Exit Cone				5. REPORT DATE January 1986	
				6. PERFORMING ORGANIZATION CODE	
7. AUTHOR(S) Roy M. Sullivan				8. PERFORMING ORGANIZATION REPORT #	
9. PERFORMING ORGANIZATION NAME AND ADDRESS George C. Marshall Space Flight Center Marshall Space Flight Center, Alabama 35812				10. WORK UNIT NO. M-508	
				11. CONTRACT OR GRANT NO.	
				13. TYPE OF REPORT & PERIOD COVERED Technical Paper	
12. SPONSORING AGENCY NAME AND ADDRESS National Aeronautics and Space Administration Washington, D.C. 20546				14. SPONSORING AGENCY CODE	
15. SUPPLEMENTARY NOTES Prepared by Structures and Propulsion Laboratory, Science and Engineering Directorate.					
16. ABSTRACT <p>This report documents the hydroburst test of the aft portion of the PAM-D exit cone. The test fixture, test instrumentation, and test procedure are described in detail. The hydrostatic pressure required to buckle the cone was recorded at 9.75 psi.</p> <p>Meanwhile, the PAM-D exit cone was modeled using the finite element method and a theoretical buckling pressure (8.76 psi) was predicted using the SPAR finite element code. This report discussed the modeling technique which was employed.</p> <p>By comparing the theoretical to predicted critical pressures, this report verifies the modeling technique and calculates a material knockdown factor for the carbon-carbon exit cone.</p>					
17. KEY WORDS Nozzle Exit Cone Hydroburst Test			18. DISTRIBUTION STATEMENT  Until January 1988 Subject Category 15		
19. SECURITY CLASSIF. (of this report) Unclassified		20. SECURITY CLASSIF. (of this page) Unclassified		21. NO. OF PAGES 32	22. PRICE